MIXING AND DISPERSION CHARACTERISTICS OF TWO-PHASE JET FLOWS WITH DIFFERENT CROSS-SECTION INJECTION GEOMETRIES

A. Abdel-Hameed* and J. Bellan**
*California Institute of Technology, Pasadena, CA. 91125
**Jet Propulsion Laboratory, California Institute of Technology, Pasadena, CA. 91109

Abstract

Direct Numerical Simulations are performed of spatial, three-dimensional, jets of different inlet geometric configurations for the purpose of quantifying the dispersion characteristics of the flows. Both single phase and two-phase flow jets are considered. The two-phase flow jets consist of gas laden with liquid drops injected at the inlet. Drop evaporation ensues due both to the gaseous flow being initially unvitiated by the vapor species corresponding to the liquid drops, and to drop heating as the initial drop temperature is lower than that of the carrier gas. The conservation equations for the two-phase flow include complete couplings of mass, momentum, and energy based on thermodynamically self-consistent specification of the vapor enthalpy, internal energy and latent heat of vaporization. Inlet geometries investigated are circular, elliptic, rectangular, square and triangular. The results focus both on the different dispersion achieved according to the inlet geometry, as well as on the considerable change in the flow field due to the presence of the drops.

Introduction

It has been know for some time that single-phase flow jets with non-circular inlets are characterized by their inherent ability to entrain more fluid than those having circular inlets. The experimental studies of Gutmark et al. [5], Schadow et al. [22], Gutmark and Ho [6], Ho and Gutmark [9], Gutmark et al. [7], Hussain and Husain [10], Husain and Hussain [11] and Gollahalli et al. [2] have established numerous features of the mixing enhancement of non-circular jets. These jets were either elliptic or issued from corner-containing geometries. Their superior mixing ability was attributed to the accompanying secondary flows which result either from the curvature variation in the azimuthal direction, or from the instabilities produced by the corners through the asymmetric distribution of pressure and mean flow field. In both cases, the coherence of the jet structures is destroyed (e.g. Schadow et al. [22]), resulting in larger mixing. For elliptic jets, azimuthal curvature variation of vortical structures produces non-uniform self-induction and three-dimensional structures resulting in spreading rates becoming larger in the minor axis plane compared to the major axis, producing axis switching. Depending on the specific corner-containing geometry, the axis switching phenomenon might not necessarily happen (equilateral triangle inlets display axis switching, but square ones do not), however, the corners promote the formation of fine-scale turbulence which enhances mixing. These experimental results were confirmed by a large number of numerical predictions. Examples of such computational studies are those of Koshigoe et al. [13], [14], Grinstein and DeVore [3], Tam and Thies [25], Husain and Hussain [12] and Miller et al. [15]. All these studies were devoted to single-phase flows. In contrast, the present investigation is devoted to two-phase flows. The intention here is to exploit the superior mixing characteristics of non-circular jets as a means of enhancing spray dispersion and furthermore mixing of the evaporated species with the ambient gas.

The paper is organized as follows: We first recall some aspects of the formulation of Miller and Bellan [17], [18] and highlight the differences in the modeling of the heat and mass fluxes between the present formulation and the aforementioned work. Furthermore, we briefly explain the departures in the treatment of boundary conditions between the confined shear layer investigated in the previous studies and the present investigation of a free jet. The initial conditions are documented next. Results, particularly those documenting the differences between single-phase jets and two-phase jets are then discussed. Finally, in the last section we state our conclusions and make recommendations for further investigations.

Model

The mathematical description of two-phase flows has followed two distinct methods. The first, mainly reserved for dilute flows (i.e. small condensed phase volume fraction), is the Eulerian - Lagrangian method whereby the gas is described in the frame of the observer (i.e. Eulerian frame) and the condensed particles are followed on their trajectories (i.e. Lagrangian frame). In the other method, both gas and condensed phase are considered as continuum flows, and they are both followed in the Eulerian frame. The present approach adopts the former technique, emulating the study of Miller and Bellan [17], [18] in the context of mixing layers. The conservation equations are solved by the technique of Direct Numerical Simulation (DNS) originally introduced for single-phase flows, and meaning that all length and time scales of the flow are resolved without resorting to either time averaged or subgrid turbulence models. In this respect,

even the present single-phase flow simulations are different from those of Grinstein and DeVore [3], Grinstein and Kailasanath [4] and Miller et al. [15], which all contained numerical dissipation that acted akin to subgrid fluctuations.

In the realm of two-phase flows the term DNS has been coined by Squires and Eaton [23], [24], to mean that all length scales of the flow are resolved, but that the condensed phase particles are treated as point sources. This terminology reflects the current impossibility, due to computer memory and computational time constraints, of solving the exact equations inside the drops and in their immediate vicinity when tracking a very large number of drops (e.g. $\sim O(10^5) - O(10^6)$), even if the calculations are performed in a small domain and for a relatively small (~ 400) Re_0. This situation leads to assuming the drops much smaller than the Kolmogorov scales, η_K, and treating them as point forces and sources. Additional to the point source assumption, other restrictions are here imposed to make the problem computationally tractable: (i) the drops are spherical, (ii) the ensemble of drops has negligible volume fraction, (iii) there are no interactions among drops, and (iv) there is no drop collision, breakup, or coalescence. The gas phase equations are completely coupled to the equations for the drops in that mass, momentum and energy are exchanged between the two phases. To describe a single drop evolution, we adopt the validated model of Miller et al. [16]. In this model, the momentum coupling between drops and flow occurs through the drag force (i.e. Basset history, added mass, lift, Magnus and other forces are neglected), and the internal droplet temperature is uniform with heat transfer to the drop occurring through convection and conduction.

Gas phase conservation equations

The compressible form of the governing equations for the gas phase, including mass, momentum and energy coupling are

$$\frac{\partial(\rho_G)}{\partial t} + \frac{\partial[\rho_G u_j]}{\partial x_j} = S_I, \tag{1}$$

$$\frac{\partial(\rho_G u_i)}{\partial t} + \frac{\partial[\rho_G u_i u_j + p_G \delta_{ij} - \tau_{ij}]}{\partial x_j} = S_{II,i}, \tag{2}$$

$$\frac{\partial(\rho_G E_G)}{\partial t} + \frac{\partial[(\rho_G E_G + p_G)u_j - q_j - u_i \tau_{ij}]}{\partial x_j} = S_{III}, \tag{3}$$

$$\frac{\partial(\rho_G Y_V)}{\partial t} + \frac{\partial[\rho_G Y_V u_j - J_{Vj}]}{\partial x_j} = S_I, \tag{4}$$

$$p_G = \rho_G R_u \left[\frac{Y_V}{W_V} + \frac{(1-Y_V)}{W_C}\right] T_G, \tag{5}$$

where q_j is the heat flux, J_{Vj} is the molar flux, ρ_G is the gas phase density, u_i is the gas phase velocity, p_G is the thermodynamic pressure, T_G is the gas temperature, τ_{ij} is the viscous stress tensor (with viscosity μ_G), $E_G = e_G + \frac{1}{2}u_i u_i$ is the total gas energy (internal e_G and kinetic $\frac{1}{2}u_i u_i$), and Y_V is the mass fraction of the evaporated liquid species. Also, W denotes the molecular weight, δ_{ij} is the Kronecker delta function, and R_u is the universal gas constant. The right-hand side terms S_I, $S_{II,i}$ and S_{III} are the coupling terms between the gas and the condensed phase, to be discussed below. Subscripts C and V refer to the carrier gas and the vapor emitted by the drops, respectively.

Individual droplet conservation equations

The Lagrangian equations describing the transient displacement (X_i), velocity(v_i), temperature (T_d) and mass (m_d) of a single droplet are those derived by Miller and Bellan, 1999:

$$\frac{dX_i}{dt} = v_i, \tag{6}$$

$$\frac{dv_i}{dt} = \frac{F_i}{m_d} = \frac{f_1}{\tau_d}(u_i - v_i), \tag{7}$$

$$\frac{dT_d}{dt} = \frac{Nu}{3\,\mathrm{Pr}_G}\left(\frac{C_{p,G}}{C_L}\right)\left(\frac{f_2}{\tau_d}\right)(T_G - T_d) + \left(\frac{\dot{m}_d}{m_d}\right)\frac{L_V}{C_L}, \tag{8}$$

$$\dot{m}_d \equiv \frac{dm_d}{dt} = -\frac{Sh}{3Sc_G}\left(\frac{m_d}{\tau_d}\right)\ln[1 + B_M], \tag{9}$$

where the subscript d denotes individual drop conditions, ρ_L is the liquid density, m_d is the drop mass, the droplet time constant for Stokes flow is $\tau_d = \rho_L D^2/(18\mu_G)$ with D being the droplet diameter, Q is the heat transfer rate to the drop which is driven by the local difference in temperature between drop and gas, C_L is the heat capacity of the liquid, whereas L_V is the latent heat of evaporation. The gas mixture heat capacity is calculated as $C_{p,G} = (1 - Y_V)C_{p,C} + Y_V C_{p,V}$, where $C_{p,C}$ and $C_{p,V}$ are the heat capacities of the carrier gas and vapor, respectively. The gas phase Prandtl and Schmidt numbers are $\mathrm{Pr}_G = \mu_G C_{p,G}/\lambda_G$ and $Sc_G = \mu_G/(\rho_G \Gamma_V)$. The drag force is driven by the local slip velocity vector $u_{sl,i} = u_i - v_i$ and the Stokes drag in eq. 7 is empirically corrected for finite droplet Reynolds numbers; basically, f_1 is function of a slip velocity based Reynolds number and a 'blowing' Reynolds number related to the velocity of the mass evaporated from the drop; see [17]. The Nusselt (Nu) and Sherwood (Sh) numbers are empirically modified for convective corrections to heat and

mass transfer based on the Ranz-Marshall correlations; see [17] for details. The function $f_2 = \beta/(e^\beta - 1)$ is an analytical evaporative heat transfer correction to the solid sphere Nusselt number, where the non-dimensional evaporation parameter β, given by

$$\beta = -\left(\frac{3\,\mathrm{Pr}_G\,\tau_d}{2}\right)\frac{\dot{m}_d}{m_d} = -\left(\frac{\rho_L\,\mathrm{Pr}_G}{8\mu_G}\right)\frac{dD^2}{dt}, \tag{10}$$

is constant for drops obeying the 'D^2 law' (see [16]).

Source terms

The phase-coupling terms appearing in eqs. 1 - 4 are

$$S_I = -\sum_\alpha \left\{\frac{w_\alpha}{\Delta V_\alpha}\left[\dot{m}_d\right]_\alpha\right\}, \tag{11}$$

$$S_{II,i} = -\sum_\alpha \left\{\frac{w_\alpha}{\Delta V_\alpha}\left[F_i + \dot{m}_d v_i\right]_\alpha\right\}, \tag{12}$$

$$S_{III} = -\sum_\alpha \left\{\frac{w_\alpha}{\Delta V_\alpha}\left[v_i F_i + Q + \dot{m}_d\left(\frac{v_i v_i}{2} + h_{V,s}\right)\right]_\alpha\right\}, \tag{13}$$

where $h_{V,s}$ is the evaporated vapor enthalpy at the droplet surface, and the drag force F_i, Q and $\dot{m}_d$ are specified by the modeled droplet conservation equations, eqs. 7 - 9. The summations are over all droplets residing within a local numerical discretization volume ΔV_α and employ a geometrical weighting factor, w_α which is used to proportionally distribute the individual droplet contributions to the eight nearest neighbor surrounding grid points (i.e., corners of the computational volume ΔV_α) according to the respective distance of the drop from the corners of the computational volume.

Fluxes, internal energy and latent heat

According to Hirshfelder et al. [8], the general form of the molar and heat fluxes, in absence of Soret and Dufour effects (here neglected, owing to the atmospheric pressure conditions), is

$$J_{Vj} = -\rho Y_V\left[\frac{\Gamma_G}{Y_V}\frac{\partial Y_V}{\partial x_j} + Y_C\left(Y_V + Y_C\frac{m_V}{m_C}\right) \times \left[\frac{m_C}{m_V} - 1\right]\frac{\Gamma_G}{p}\frac{\partial p}{\partial x_j}\right], \tag{14}$$

$$q_j = -\lambda_G\frac{\partial T_G}{\partial x_j} + \left(h_V - h_C\right)J_{Vj}, \tag{15}$$

where Γ_G and λ_G are the Fickian diffusion coefficient and the constant gas phase thermal conductivity, respectively. Here h_C and h_V are the enthalpies of the pure gases

$$h_C = C_{p,C}T_G, \qquad h_V = C_{p,V}T_G + h_V^0, \tag{16}$$

with the mixture enthalpy defined by

$$h = e + p/\rho = C_pT + h_V^0 Y_V = h_C Y_C + h_V Y_V. \tag{17}$$

We note that the present formulation, due to Okong'o and Bellan [20], is more general than that of Miller and Bellan [17], [18], in that here the pressure gradient term in eq. 14 and the enthalpy carried by the molar fluxes term in eq. 15 are included. Although the pressure gradient term may be very small, and as a result has been neglected in the calculations below, the enthalpy carried by the molar fluxes may rival the thermal conductivity term under low T_G conditions such as those studied herein (see Okong'o and Bellan [20]).

For thermally perfect species and calorically perfect gas (i.e. constant heat capacities at constant pressure)

$$h_{V,s} = C_{p,V}T_d + h_V^0, \tag{18}$$

$$L_V = h_V^0 - (C_L - C_{p,V})T_d, \tag{19}$$

$$e_G = (1 - Y_V)[C_{v,C}T_G] + Y_V[C_{v,V}T_G + h_V^0]. \tag{20}$$

The drop temperature is uniform due to the assumption of infinite liquid thermal conductivity, and thus $T_{d,s} = T_d$.

Using the above definitions, the phase coupling terms may now be expressed as:

$$S_I = -\sum_\alpha \left\{\frac{w_\alpha}{\Delta V_\alpha}\left[\frac{d}{dt}(m_d)\right]_\alpha\right\}, \tag{21}$$

$$S_{II,i} = -\sum_\alpha \left\{\frac{w_\alpha}{\Delta V_\alpha}\left[\frac{d}{dt}(m_d v_i)\right]_\alpha\right\}, \tag{22}$$

$$S_{III} = -\sum_\alpha \left\{\frac{w_\alpha}{\Delta V_\alpha}\left[\frac{d}{dt}(m_d C_L T_d + \frac{1}{2}m_d v_i v_i)\right]_\alpha\right\}, \tag{23}$$

where the time derivatives express the total rates of change of the individual drop mass, momentum and total energy, respectively.

Boundary conditions

The adopted boundary conditions are based on the Navier-Stokes Characteristic Boundary Conditions derived by Baum et al. [1], similar to [17]. Compared to the studies of [17], [18] and [19], the present simulations are of a 3D free, viscous subsonic jet flow. In this situation, there is one inflow boundary at $x_1 = 0$, and the other five boundaries conditions are of type outflow. For physical consistency and well-posedness, the Euler equations (on which the relationships of [1] are based), must have six boundary conditions at the inflow. Threfore, we the

impose the value of the gas density, the vapor mass fraction and the three components of the velocity. The additional 'numerical' or 'soft' boundary condition is found from the energy equation. At the outflow boundaries, we chose subsonic non-reflecting boundary conditions. For the Euler equations, it is sufficient to impose the pressure at infinity, p_∞ [1]. To complete the boundary conditions with the viscous conditions necessary for the NS equations, here we chose the normal derivative of the tangential stresses, the normal heat flux, and the normal vapor mass fraction flux to be all null.

At corners, the imposed boundary conditions in a given direction are consistent with the direction of the flow, being either inflow or outflow.

Flow configuration and initial conditions

The geometric configuration is illustrated in Fig. 1 for the special case of a circular inlet, and the coordinates x_1, x_2, and x_3 are defined. The computational domain dimensions are $L_1 = 2L_2 = 2L_3 = 8d_J = 0.16m$. The equivalent jet diameter d_J (which is the diameter of the circle that has the same area as the non-circular inlet sections) is chosen to be 0.02 m for all geometrical configurations. The Mach number is defined as

$$M = U_0/\sqrt{R_u T_{G,0} C_{p,C}/(W_C C_{v,C})} \qquad (24)$$

where the jet Mach number, $M_J = 0.35$, is based on $U_0 = U_J$, and the ambient Mach number, $M_\infty = 0.05$, based on U_∞. The velocity $U_J = 131$ m/s is the constant inlet gas velocity, being determined from the specified value of M_J, and $U_\infty = 18.7$ m/s is the constant gas velocity in the freestream, being determined from the specified value of M_∞. To avoid a spatial discontinuity, the two disparate velocities are connected through a tanh function with a width of $d_J/25$ in the direction of initial discontinuity, x_2. In eq. 24, $T_{G,0}$ is the initial gas temperature and $C_{v,C}$ is the carrier gas heat capacity at constant volume.

The initial jet Reynolds number, $\mathrm{Re}_J = \rho_{G,0}\Delta U_0 d_J / \mu_G = 500$, where $\Delta U_0 = U_J - U_\infty$. The initial flow field is isobaric with $p_0 = p_{atm}$, and isothermal with $T_{G,0} = 400$ K, and $\rho_{G,0} = 1$ kg/m^3. The droplets are inserted into the domain, randomly distributed and with velocity $v = \sqrt{v_1^2 + v_2^2 + v_3^2} = 0.75U_J$, through the jet orifice. The drop size is uniform (portraying a monodisperse spray), with initial diameter of $50\mu m$ and initial temperature $T_{d,0} = 300$ K. The mass flow rate of liquid is 0.012 kg/s and the mass loading, representing the ratio of liquid to air mass, is $ML = 0.29$.

The two species chosen for this study are air for the carrier gas and decane for the liquid /vapor hydrocarbon. Initially, the freestream mass fraction of the evaporated species is null, and the equivalent value in the jet is 0.03; a tanh function of same width as that of the initial velocity profile is used to avoid a spatial discontinuity in the mass fraction. All heat capacities, the gas Prandtl number and vapor reference enthalpy are evaluated at 400 K. The Lewis number (Le_G) is assumed to be unity (i.e. $Sc_G = \mathrm{Pr}_G$). The gas phase viscosity is determined through the specification of Re_J. Due to the enlarged viscosity value inherent in all DNS calculations, the species can be labeled 'pseudo-air' and 'pseudo-decane'; however, effects due to realistic air-hydrocarbon molecular weight ratios, heat capacity ratios and latent heat magnitude are retained herein. The constant property values used in the simulations are provided in Table 1.

The general numerics discussed in detail in [17] and [18] is used here with minute changes. All simulations are performed on a SGI Origin 2000 parallel supercomputer using 32 processors with a $8 \times 2 \times 2$ spatial decomposition. In all simulations the uniform grid resolution is $240 \times 180 \times 180$ in the x_1, x_2 and x_3 directions, so as to resolve the smallest scales for the specified value of Re_J.

Results

Non-circular single-phase flow jets have been studied extensively numerically, and their distinctive features are already established. However, to document their particular aspects of interest in this study, simulations of single-phase flows are here performed for the same configuration as those of the two-phase flow simulations, so as to allow meaningful comparisons. Additional to documenting the effect of the drops on the flow through comparisons of single- and equivalent two-phase flow simulations, we are also interested in exploring the different drop dispersion patterns, by illustrating the instantaneous Eulerian drop number density

$$n = \sum_\alpha \frac{w_\alpha}{\Delta V_\alpha} \qquad (25)$$

according to the inlet geometry. The drop dispersion patterns influence the distribution of the evaporated species, and thus mixing. To quantify mixing, we focus on the product thickness

$$\delta_p = \int\int\int_V \rho Y_p dV \qquad (26)$$

in mass units, where $Y_p = 2\min(Y_V, Y_C)$, is a direct consequence of molecular mixing. All these quantities will be evaluated at the non-dimensional time $t^* = t\Delta U_0 / d_j$, corresponding to the achievement of a steady-state condition based on the mass flux entering and exiting the domain, t_s^*. Moreover, it is also important to document contours of instantaneous liquid mass per unit volume, $(4\pi/3)nR^3\rho_L$, and vapor mass fraction at different streamwise locations.

As an example of the results, in Fig. 2-4 we illustrate the non-dimensional streamwise velocity distribu-

tions in several $x_2 - x_3$ planes, and the equivalent plots for the nondimansional streamwise vorticity are in Figs. 5-7. These, will be discussed and interpreted for different cross-stream section geometries.

Summary

The dispersion and mixing of liquid drops in three-dimensional circular and non-circular gaseous jets has been investigated through Direct Numerical Simulation at Reynolds numbers characteristic to pre-transitional flows. The conservation equations were formulated in an Eulerian frame for the gas and in a Lagrangian frame for the drops with two-way coupling whereby the flow influences the drops and the drops impact the flow through mass, momentum, species and energy transfer. In all simulations, drops of 50 μm diameter were randomly introduced at the inlet with null relative velocity with respect to the carrier flow. The mass flow rate of drops was the same in all simulations, as were the initial Reynolds number and the Mach number of the flow. The drop initial temperature was 300 K and the gas temperature was 400K.

To quantify the influence of the drops on the flow, a separate set of simulations were performed for the same geometric configuration and initial conditions for gaseous jets. Results from these simulations show the beneficial effect of the non-circular geometries upon drop dispersion and vorticity creation in the flow, influencing mixing.

Acknowledgment

This investigation was performed at the California Institute of Technology's Jet Propulsion Laboratory (JPL). One of the authors (H. A-H.) would like to acknowledge financial support from the Egyptian Ministry of Education, through a graduate student scholarship, during the period of this investigation. The authors would like to thank Dr. Nora Okong'o for many helpful discussions on coding aspects. The JPL supercomputer facility was used in the course of this study.

1. Baum, M., Poinsot, T. and Thévenin, D., 1994 Accurate boundary conditions for multicomponent reactive flows, J. Comp. Phys., 116, 247-261.
2. Gollahalli, S. R., Khanna, T. and Prahbu, N. 1992 Diffusion flames of gas jets issued from circular and elliptic nozzles, Comb. Sci. and Tech., 86, 267-288.
3. Grinstein, F. F. and DeVore, C. R., 1992 Coherent structure dynamics in spatially-developing square jets, AIAA-92-3441, AIAA/SAE/ASME/ASEE 28th Joint Propulsion Conference and Exhibit, July 6-8, Nashville, TN.
4. Grinstein, F. F. and Kailasanath, K., 1995 Three-dimensional numerical simulations of unsteady reactive square jets, Comb. Flame, 100, 2-10.
5. Gutmark, E., Schadow, K. C., Parr, T. P., Harris, C. K. and Wilson, K. J., 1985 The mean and turbulent structure of noncircular jets, AIAA-85-0543, AIAA Shear Flow Conference, March 12-14, Colorado Springs, CO.
6. Gutmark, E. and Ho, C-M., 1986 Visualization of a forced elliptic jet, AIAA J., 24(4), 684-685.
7. Gutmark, E., Schadow, K. C., Parr, T. P., Hanson-Parr, D. M. and Wilson, K. J., 1989 Noncircular jets in combustion systems, Experiments in Fluids, 7, 248-258.
8. Hirshfelder, J. O., Curtis, C. F. and Bird, R. B., 1954 *Molecular theory of gases and liquids,* John Wiley & Sons, Inc., 516, 717.
9. Ho, C-M. and Gutmark, E., 1987 Vortex induction and mass entrainment in a small-aspect-ratio elliptic jet, J. Fluid Mech., 179, 383-405.
10. Hussain, F. and Husain, H. S., 1989 Elliptic jets. Part 1. Characteristics of unexcited and excited jets, J. Fluid Mech., 208, 257-320.
11. Husain, H. S. and Hussain, F., 1991 Elliptic jets. Part 2. Dynamics of coherent structures: pairing, J. Fluid Mech., 233, 439-482.
12. Husain, H. S. and Hussain, F., 1993 Elliptic jets. Part 3. Dynamics of preferred mode coherent structure, J. Fluid Mech., 248, 315-361.
13. Koshigoe, S., Gutmark, E., Schadow, K. C. and Tubis, A., 1988a Instability analysis on non-circular free jets, AIAA-88-0037, AIAA 26th Aerospace Sciences Meeting, January 11-14, Reno, NV.
14. Koshigoe, S., Gutmark, E., Schadow, K. C. and Tubis, A., 1988 Wave structures in jets of arbitrary shape. III Triangular jet, Phys. Fluids, 31(6), 1410-1419.
15. Miller, R. S., Madnia, C. K. and Givi, P., 1995 Numerical simulation of non-circular jets, Computers and Fluids, 24(1), 1-25.
16. Miller, R. S., Harstad, H. G. and Bellan, J., 1998 Evaluation of equilibrium and non-equilibrium evaporation models for many droplet gas-liquid flow simulations, Int. J. of Multiphase Flow, 24, 1025-1055.
17. Miller, R. S. and Bellan, J., 1999 Direct Numerical Simulation of a confined three-dimensional gas mixing layer with one evaporating hydrocarbon-droplet laden stream, J. Fluid Mech., 384, 293-338.
18. Miller, R. S. and Bellan, J., 2000 Direct Numerical Simulation and subgrid analysis of a transitional droplet laden mixing layer, Physics of Fluids, 12(3), 650-671.
19. Okong'o, N. and Bellan, J., 2000 A priori subgrid analysis of temporal mixing layers with evaporating

droplets, Physics of Fluids, 12(6), 1573-1591.

20. Okong'o, N. and Bellan, N., 2001, Dynamic subgrid scale modeling of a mixing layer laden with evaporating drops, in preparation.
21. Sangiovanni, J. J. and Liscinsky, D. S., 1985, Soot formation characteristics in well-defined spray flames, Proc. of the Comb. Institute, 20, 1063-1073.
22. Schadow, K. C., Wilson, K. J., Parr, D. M., Bicker, C. J. and Gutmark, E., 1985 Reduction of flow coherence in forced subsonic jets, AIAA-85-1109, AIAA /SAE/ASME/ASEE 21st Joint Propulsion Conference and Exhibit, July 8-10, Monterey, CA.
23. Squires, K. D. and Eaton, J. K., 1990 Particle response and turbulence-modification in isotropic turbulence, Phys. Fluids A, 2(7), 1191-1203.
24. Squires, K. D. and Eaton, J. K., 1991 Preferential concentration of particles by turbulence, Phys. Fluids A, 3(5), 1169-1178.
25. Tam, C. K. W. and Thies, A. T., 1993 Instability of rectangular jets, J. Fluid Mech., 248, 425-448.

Property	Value
W_C	28,97 kg/kg mole
W_V	142.0 kg/kg mole
$C_{p,C}$	1006.24 J/(kg K)
$C_{p,V}$	1980 J/(kg K)
C_L	2520.5 J/(kg K)
Pr_G	0.695
ρ_L	642 kg/m^3
$T_{B,L}$	447.7 K
h_V^0	5.2×10^5 J/K

Table 1: Properties used in the simulations (evaluated at atmospheric pressure and T=400 K from correlations for air and decane found in Miller et al., 1998). The subscripts L, C and V denote the liquid, carrier gas and evaporated vapour, respectively.

Run	Geometry	Aspect ratio
1s, 1t	circular	1:1
2s, 2t	elliptic	2:1
3s, 3t	square	1:1
4s, 4t	rectangular	2:1
5s, 5t	triangular	1:1

Table 2: Geometries for the single (s) and two-phase (t) flow simulations.

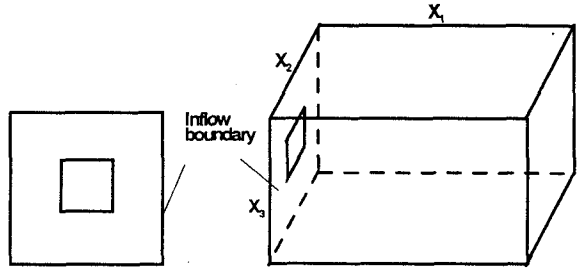

Figure 1: Physical configuration for a square cross-section spray.

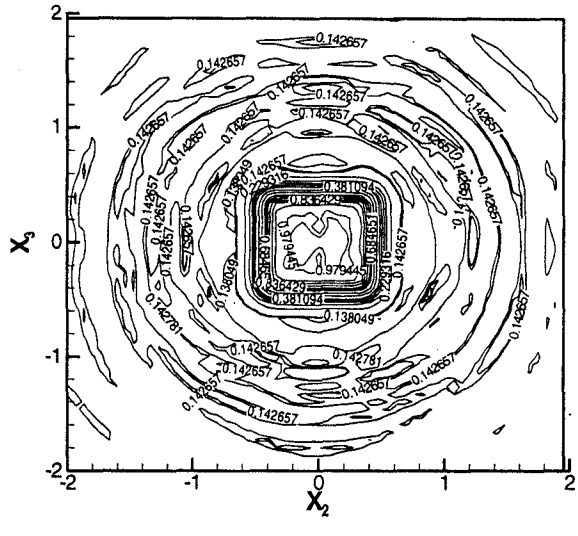

Figure 2: Non-dimensional velocity, u_1/U_J for the square jet at $x_1/d_J = 0$.

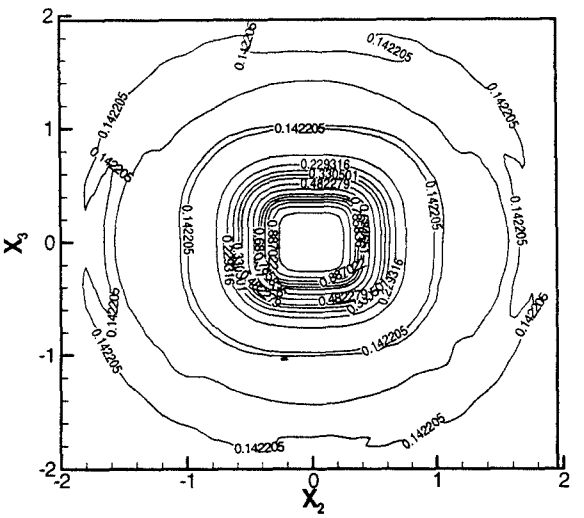

Figure 3: Non-dimensional velocity, u_1/U_J for the square jet at $x_1/d_J = 2.5$.

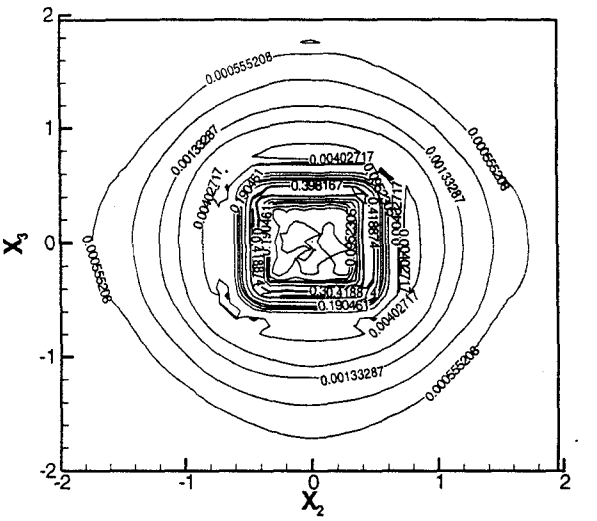

Figure 5: Non-dimensional vorticity, $\omega_1/\omega_{\max}$ for a square jet at $x_1/d_J = 0$. $\omega_{\max}$ is the maximum vorticity in the domain.

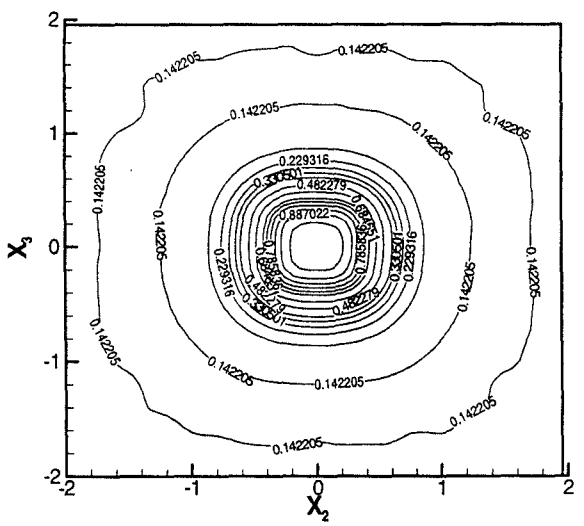

Figure 4: Non-dimensional velocity, u_1/U_J for the square jet at $x_1/d_J = 5$.

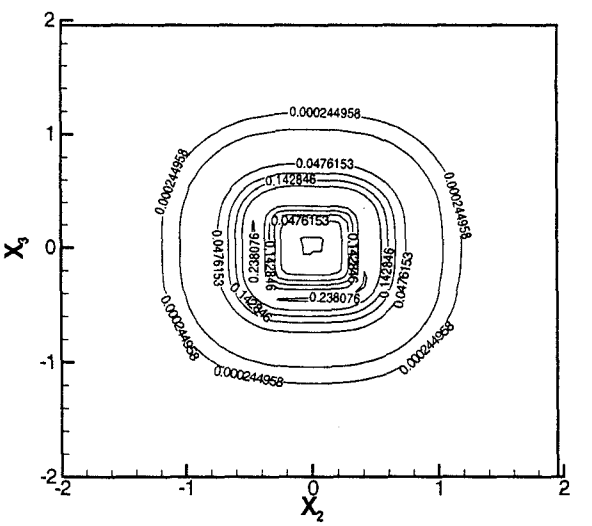

Figure 6: Non-dimensional vorticity, $\omega_1/\omega_{\max}$ for a square jet at $x_1/d_J = 2.5$. $\omega_{\max}$ is the maximum vorticity in the domain.

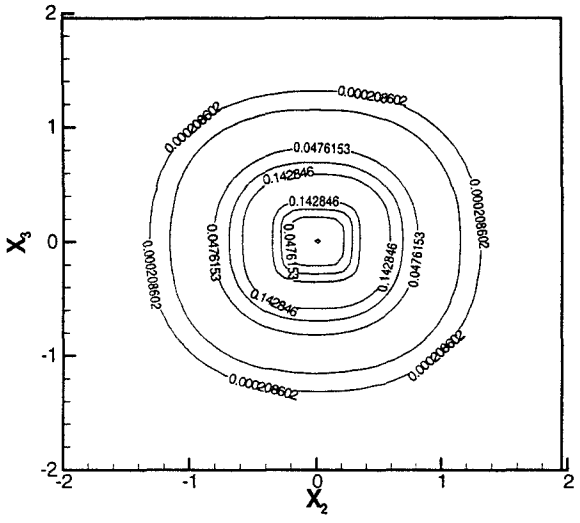

Figure 7: Non-dimensional vorticity, $\omega_1/\omega_{\max}$ for a square jet at $x_1/d_J = 5$. $\omega_{\max}$ is the maximum vorticity in the domain.